Journal of the Physical Society of Japan
Vol. 79, No. 12, December, 2010, 124502

Controlled Extraction of Ultracold Ions from a Linear Paul Trap for Nanobeam Production

Kenji IZAWA*, Kiyokazu ITO, Hiroyuki HIGAKI, and Hiromi OKAMOTO

Graduate School of Advanced Sciences of Matter, Hiroshima University, 1-3-1 Kagamiyama, Higashihiroshima, Hiroshima 739-8530, Japan

(Received May 31, 2010; accepted September 21, 2010; published December 10, 2010)

At ultralow temperatures near absolute zero, a small number of ions confined in a linear Paul trap align along the trap axis forming a string Coulomb crystal. The emittance of an ideal Coulomb crystal is close to zero, which implies that the Paul trap can be a unique source of extremely high quality ion beams. In this paper we address the results of proof-of-principle experiments that demonstrate the feasibility of the nondestructive extraction and acceleration of string Coulomb crystals from a conventional linear Paul trap for nanobeam production. The Doppler laser-cooling technique is employed first to crystallize a few $^{40}Ca^{+}$ ions and, then, the DC potentials on the end electrodes are switched to launch the ions from the trap. It is confirmed that ultracold ions can be extracted without serious heating. The time interval of adjacent ions and their arrival time at the detector are controllable by changing the electrode potential. Three-dimensional multiparticle simulations are also carried out, which explain the experimental observations fairly well.

KEYWORDS: nanobeam, ion source, linear Paul trap, Coulomb crystal, laser cooling
DOI: 10.1143/JPSJ.79.124502

1. Introduction

Charged particle beams have been employed as a useful tool in a wide variety of fields including fundamental and applied physics, material sciences, life sciences, coherent light generation, industry, and medicine. The typical beam conditions required for individual fields are rather different. While modern physics experiments often demand very high-energy and high-intensity beams, this is not the case in most of the other applications. In particular, recent interest in radiation effects on diverse objects has considerably enhanced the importance of low-current *microbeams* that allow extremely localized irradiation of particles onto targets. Such tiny beams can be used, for instance, to investigate radiation-induced damage to living cells and their responses.[1–3] The so-called "single event upset (SEU)" caused in electronic devices by cosmic rays is another subject that can be studied systematically with the help of microbeams.[4] We can apply well-focused ion beams to secondary ion-microprobe mass spectrometry, micromachining, lithographic mask repair, and semiconductor production in addition to radiation damage studies.[5–10] It is even possible to carry out complex doping of multiple ions at a specific depth, provided that the beam quality is sufficiently high.[11]

Ion beams employed for these particular purposes have been produced typically by applying a high electric field to a liquid metal or by using multicusp ion sources.[5–11] In any case, we need to collimate the beam with microapertures and strongly focus it before the target because the initial beam *emittance* is not sufficiently low.[12] If the beam energy required is in a MeV range or much higher, we have to accelerate the ions, which considerably deteriorates the beam quality in general. High-energy ion beams from cyclotrons and other types of accelerators are usable, but we still need subsequent systems to eventually reduce the beam size to a submicron order.[1,2,13,14]

In this paper, we experimentally study an alternative approach to attaining a low-current nanobeam. All the conventional systems mentioned above manipulate beams *after* they come out from certain ion sources. In contrast, the present method is based on the idea of manipulating ions *before* they are extracted from the source. Since the transverse size of a charged-particle beam is proportional to the square root of its emittance, the best way for micro- or nano-beam production is to make the initial emittance as low as possible. If an extremely low emittance is available, the transverse beam size can be kept small throughout the transport channel, while a conventional well-focused beam immediately diverges before and after the focal point.

The novel ion source considered here exploits an ordinary "linear Paul trap" (LPT) equipped with a laser-cooling system.[15] Ions of a specific species are confined in the LPT and cooled with an axial laser to temperature near absolute zero where the single-species ion plasma reaches a Coulomb crystalline state.[16–18] When the line density of the plasma is below a certain threshold, the crystalline structure is the so-called "string" in which all ions align along the trap axis at equal intervals.[19] The emittance of a Coulomb crystal is close to the ultimate limit, which means that an ion beam with the highest possible quality becomes available if we can launch the crystal from the trap maintaining its ordered configuration. The use of a LPT as an ion source was previously discussed not only for nanobeam production,[20,21] but also for highly charged ion beam production.[22] Recently, Schnitzler *et al.* have succeeded in accelerating a few ultracold ions laser-cooled in a LPT.[23] This seminal proof-of-principle experiment was performed with a unique, segmented LPT to minimize the possible radial heating of the ions during the axial extraction.

In the present experimental study, we employ an ordinary LPT and show that it is still possible to achieve the nondestructive extraction of a linear ion chain. We also demonstrate that the axial velocity and spacing of the ions at

*E-mail: kizawa-038@hiroshima-u.ac.jp

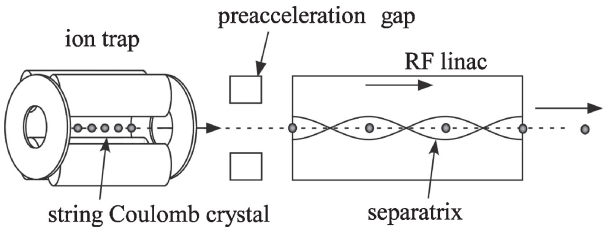

Fig. 1. Concept of the ultralow-emittance beam generator. A string Coulomb crystal is extracted from a linear Paul trap and goes through a DC acceleration gap to gain the desired kinetic energy. In the case that a much higher energy is required, the crystal is further accelerated by an rf linac. Since each individual ion can, in principle, be placed very close to the stable fixed point of the rf separatrix, the heating effect from the strong rf accelerating field is almost suppressed.

the extraction are controllable. Although the maximum current obtained in a single shot is limited in this scheme and much lower than those of conventional microbeams, the transverse beam extent can be on the nano-order level in principle.[23] Such an ultralow intensity nanobeam is particularly useful for the systematic studies of SEU, the bystander effect, etc., where we need to strike a tiny target with not many ions but just a single ion. The concept of the ultralow-emittance beam generator is schematically explained in Fig. 1. All information, such as the precise number of ions running and exactly when they are arriving at the target, is known in advance. Another important fact is that we can accelerate the ion chain to an arbitrary high energy without major longitudinal heating. Since the time interval between any two adjacent ions is almost identical and controllable, it is possible to put individual ions near the stable fixed points of the rf separatrices of the postaccelerator.[24] Then, only little rf heating occurs during acceleration because the ions never execute large synchrotron oscillations. Note further that a very high operating rf frequency can be chosen, which makes the accelerating structure unusually compact and the shunt impedance extremely high. Since the beam emittance is very low from the beginning, no final focusing system is necessary.

In §2, detailed descriptions are given of the experimental apparatus applied to the present study. Section 3 is devoted to a brief explanation of the multiparticle simulation code that we developed to analyze experimental data. Measurement results are shown in §4 and compared with simulations in which the actual three-dimensional (3D) structure of the trap system is incorporated. We address the generation of Coulomb crystals by laser cooling and results of crystal extraction experiments. Concluding remarks are finally given in §5.

2. Experimental Apparatus

A schematic of our experimental system is shown in Fig. 2. The main components include a conventional four-rod-type LPT (see Fig. 3), a vacuum system, a laser cooler, an intensified charge coupled device (ICCD) camera for laser-induced fluorescence (LIF) measurements, and a microchannel plate (MCP) for detecting individual ions from the trap. The spatial resolution of the ICCD, which has 512×512 pixels and a dynamic range of 12 bits, is 1.9 μm. The ion species chosen for the experiments is $^{40}Ca^{+}$, which

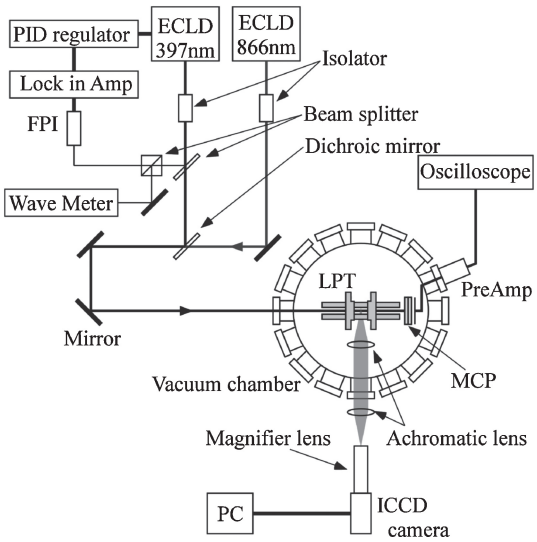

Fig. 2. Schematic of the experimental system.

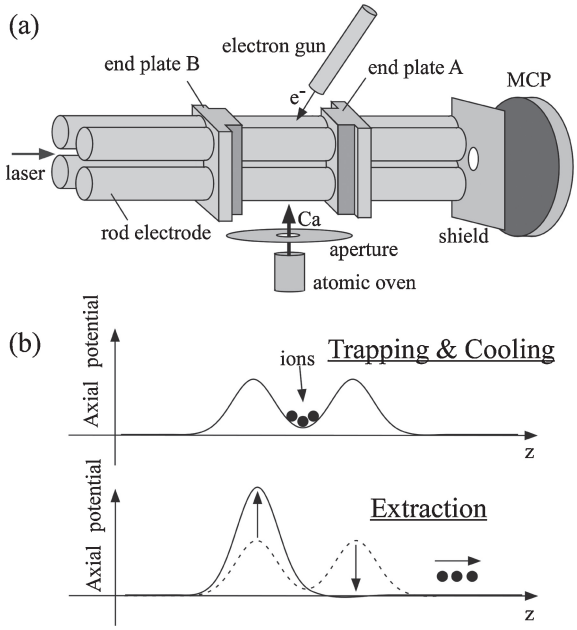

Fig. 3. (a) Schematic view of the LPT. The structure is very simple; the main components are four cylindrical rods and two end plates with a hole. The end plates are electrically isolated from the quadrupole rods and axially movable so that we can change the length of the plasma confinement region. A compact atomic oven is located below the center of the LPT. Neutral gases produced by the oven pass through a couple of apertures and are eventually ionized by an electron beam coming from an electron gun placed above the LPT. (b) Possible ion-extraction scheme. An axial potential well is maintained during the ionization and cooling processes by applying constant DC voltages on both end plates. After a Coulomb crystal is formed, the DC voltages are quickly switched to release ultracold ions along the axis.

can be cooled with compact semiconductor lasers. The resonant frequency of the cooling transition $4s^2S_{1/2}$–$4p^2P_{1/2}$ is 397 nm. Since a portion of excited ions decay to the metastable state $3d^2D_{3/2}$, we need another laser light of 866 nm to repump those ions back to the upper level $4p^2P_{1/2}$. The radiation powers generated by the external cavity laser diodes (ECLDs) here are 1.3 mW for cooling (397 nm) and 1.6 mW for repumping (866 nm).

A standard optical system was constructed to carry out Doppler laser cooling.[25,26] The frequency of the cooling laser must be controlled precisely in order to reach a value near the Doppler limit, which is 0.54 mK for $^{40}Ca^{+}$ ions. We usually fix the laser frequency f_L at a certain value to decelerate the ions. The optimum detuning is given by $\Delta f \equiv f_L - f_0 = -\Gamma/2$ where f_0 and Γ are, respectively, the resonant frequency and natural line width of the cooling transition. Γ is 22.5 MHz for $^{40}Ca^{+}$ ions and the Doppler cooling limit is defined by $T_D = \hbar\Gamma/2k_B$ where k_B and $\hbar$ are the Boltzmann constant and reduced Planck constant. The laser frequency must be stabilized with on accuracy better than Γ. As shown in Fig. 2, the laser light of 397 nm goes through a beam splitter that separates a fraction of the laser power. The fractional light is led to a wave meter for frequency monitoring and also to a thermally stabilized Fabry–Perot interferometer (FPI) whose output signal is used for feedback control of the ECLD.

Unlike the previous experiments by Schnitzler *et al.*,[23] we here employ a quite simple LPT, as shown in Fig. 3(a). This LPT was originally designed for different purposes. The four electrode rods of 6.9 mm diameter are 180 mm long and placed 3 mm apart from the trap axis. The long electrodes and thin metallic shield prevent the plasma confinement potential from being distorted by a high voltage on the MCP surface. The two end plates axially movable are currently set 6 mm apart. Low-energy electrons (<120 eV and ~0.1 mA) from an electron gun go across the center of the trap, ionizing neutral Ca gas from an atomic oven. The LPT and other components are fixed on the vacuum chamber where the base pressure of less than 5×10^{-7} Pa can be reached with a turbomolecular pump. Each excited ion quickly returns to the original level, emitting a single photon. A pair of achromatic lenses, one of which is inside the chamber and the other outside, is used to transfer these spontaneously emitted photons (LIF signals) from the ions horizontally toward the ICCD camera.

3. Numerical Simulations

We developed a multiparticle simulation code to interpret experimental data correctly. The code can analyze the 3D trajectories of ions confined in an arbitrary LPT system and Coulomb interactions. It is possible to simulate any complex experimental procedures taken in actual experiments. The numerical integration scheme is symplectic unless a nonconservative force is activated. To run the code, we first employ the commercially available software "CST STUDIO"[27] that provides 3D information on the ion confinement field generated with an arbitrary electrode geometry. Since the existence of the MCP and shield plate (see Fig. 3) may strongly affect the ion orbits, the detailed configuration of the whole system has to be input to CST STUDIO. The output 3D data of the electric fields are imported into the multiparticle code for reliable simulations. For reference, we show, in Fig. 4, an example of the potential distribution calculated using CST STUDIO with the current design of our system.

The LPT utilizes an rf quadrupole field to confine charged particles transversely. We have chosen the operating rf frequency to be 2 MHz (while it can be changed if necessary). The possible rf amplitude for stable transverse

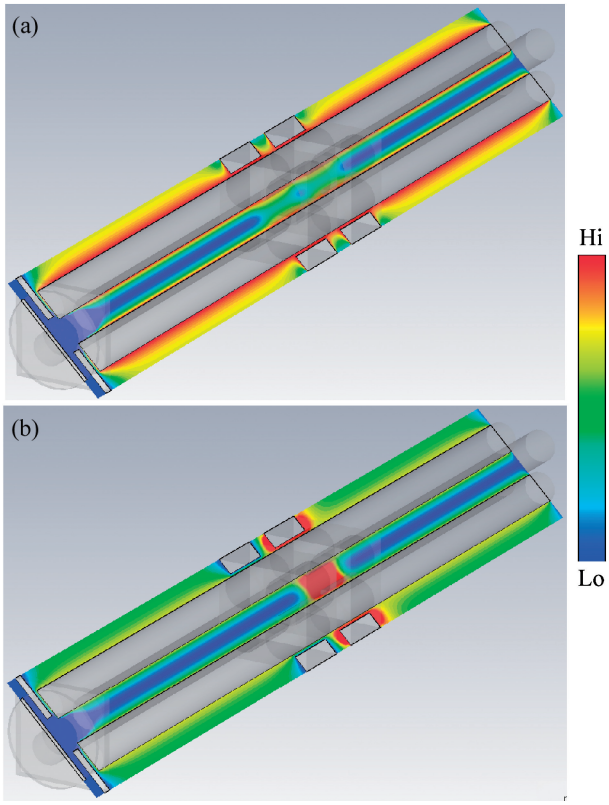

Fig. 4. (Color) Examples of electric-potential data obtained with the 3D Maxwell equation solver "CST STUDIO". The actual geometry of the experimental apparatus has been taken into account. (a) Electric potential at a certain time when ions are confined in between the end plates. (b) Field strength after the DC potentials on the end plates are switched for ion extraction. The potential height (color) varies periodically because the long electrode rods are excited with sinusoidal rf voltages all the time.

confinement of $^{40}Ca^{+}$ ions then ranges from 0 to 134 V according to the mathematical properties of the Mathieu equation. In practice, the stability of an ion plasma is influenced by Coulomb interactions especially at low temperatures and by the inevitable nonlinearity involved in the actual confinement field. It is thus desirable to choose the rf amplitude carefully, so that the plasma can be stable over the whole temperature range. In the following, the rf amplitude V_{rf} is set at 30 V whenever we laser-cool the ions.[28]

The axial ion confinement is achieved by applying DC voltages to the two end plates (see Fig. 3). We denote the end-plate voltage of the MCP side to be V_A and that of the other side to be V_B for later convenience. V_A and V_B are key parameters in the present experiments. We usually keep $V_A = V_B = 0.5$ V while cooling the ions. The ions are then stored near the bottom of the axial potential well, as illustrated in the upper picture of Fig. 3(b). The height of the potential peaks on the trap axis is somewhat lower than the DC voltages actually given to the end plates. After a string Coulomb crystal is formed, we remove the potential wall of the MCP side to release ultracold ions [see the lower picture of Fig. 3(b)]. To control the axial ion velocity at extraction, we quickly change V_B simultaneously with V_A. Figure 5 shows typical trajectories of four $^{40}Ca^{+}$ ions initially cooled to the Doppler limit. These ions forming a string crystal [Fig. 5(a)] are extracted by switching V_A and V_B to other

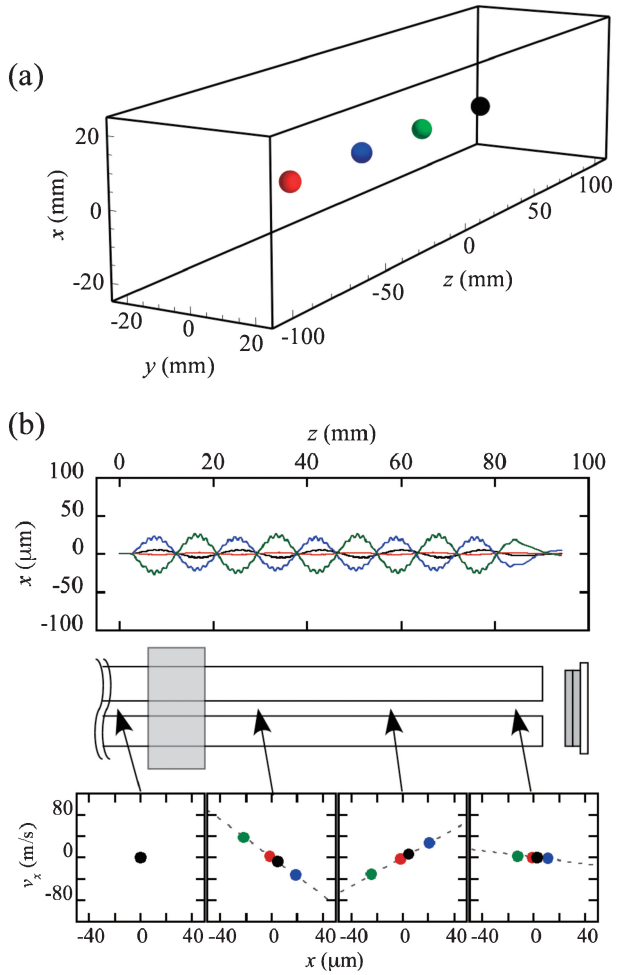

Fig. 5. (Color) Numerical example obtained with the 3D multi-particle simulation code. We have assumed the typical experimental conditions given in §3. (a) Initial distribution of four $^{40}Ca^{+}$ ions confined in the LPT and laser-cooled to the Doppler limit. (b) Transverse trajectories of the ions along the LPT and the corresponding phase-space plots at different axial positions.

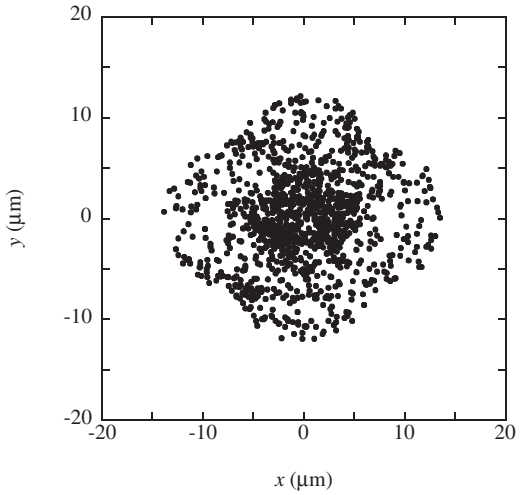

Fig. 6. Spatial distribution of extracted $^{40}Ca^{+}$ ions on MCP. We did 300 numerical simulations under the same conditions, as assumed in Fig. 5 (but with different random numbers to define the initial distribution of the four ions). Each dot represents the transverse coordinates of an ion on the MCP detector.

specific values of U_A and U_B, respectively, within 10 ns. We here simply choose $U_A = 0$, while U_B has to be a certain positive value. In Fig. 5, U_B is set at 20 V. Since the MCP located 5 mm away from the exit of the LPT is biased to -2.43 kV, all ions are eventually accelerated to that energy when arriving at the detector. No emittance growth occurs during this final acceleration by the static MCP potential. As shown in Fig. 5(b), the transverse oscillation amplitudes of some ions grow to over 10 μm while they are transported through the LPT. This is, however, not essential at all; what really matters is not the spatial amplitude but the emittance of the beam. Figure 5(b) indicates that the four ions are always on a straight line in the transverse phase space, which means that the emittance is kept very small after the extraction procedure. The distribution of extracted ions on the MCP surface is plotted in Fig. 6. The standard deviation of the distribution is about 5 μm, which can be further reduced with simple focusing lenses if required. The transverse velocity distribution has an average standard deviation of 57 m/s. Since the axial velocity is about 10^5 m/s due to the acceleration by the MCP field, the transverse divergence is less than 10^{-3} radians. The normalized rms emittance is then on the order of 10^{-13} m far below those of ordinary ion beams. If we accelerate the beam to a higher energy, the transverse beam size naturally decreases because of the so-called adiabatic damping.[29] Ideally, the beam size becomes ten times smaller at a kinetic energy of 24.3 MeV in the present case (without any elaborate final focusing system).

The normalized emittance of an ordinary heavy-ion beam from an ordinary ion source is typically around 10^{-6} m, which is seven orders of magnitude greater than that of the present ultracold beam. The use of collimators and/or final focusing lenses is, therefore, inevitable to reduce the beam spot size to a micron order. Assuming an initial beam size to be a few mm, the transverse emittance could be lowered by a factor of 10^{-4} after passing through a dedicated collimation system; then, the resultant emittance is on the order of 10^{-10} m. Even if the collimation efficiency is ten times better (i.e., 10^{-5} instead of 10^{-4}), the final emittance is still far above 10^{-13} m.

Note that the normalized transverse emittance of 10^{-13} m, which is exceptionally low, is inconsistent with the temperature of an ideal Coulomb crystal. If $^{40}Ca^{+}$ ions are cooled to the Doppler limit (0.54 mK), the corresponding emittance should even be much lower. This suggests that some heating has occurred after the switch of the end-plate potentials. The most likely source of the emittance growth is interparticle Coulomb interactions when the ultracold ions start to move toward the exit of the trap (because the ions are still tightly spaced at the beginning). 3D numerical simulations have actually revealed that the emittance rapidly grows in the vicinity of the end plate A. We have also found that the growth rate increases as the extraction voltage U_B is set higher. The average normalized emittance at the MCP position is plotted in Fig. 7 as a function of U_B. It is now evident that a lower U_B is preferred in our system to minimize the undesirable beam-quality deterioration. The achievable transverse emittance can be less than 10^{-14} m if we choose U_B of a few volts. When the number of ions

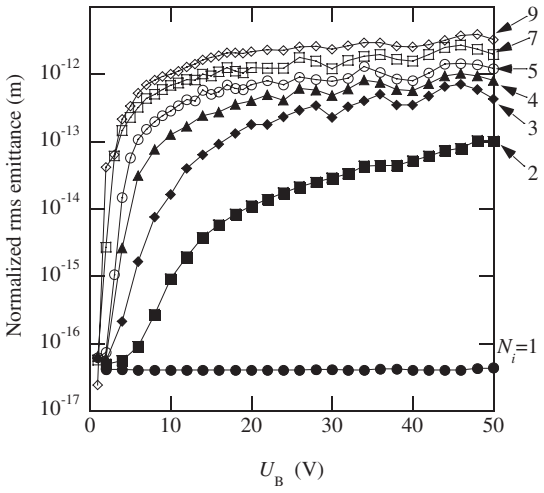

Fig. 7. U_B dependence of normalized transverse rms emittances at the MCP position. We performed many 3D simulations varying U_B and the number of ions forming a string Coulomb crystal. In each choice of experimental parameters, 50 independent simulation runs are carried out to evaluate the average rms emittance at the MCP. The initial ion number N_i is changed from 1 to 9 (above which the crystal is transformed to the zigzag configuration).

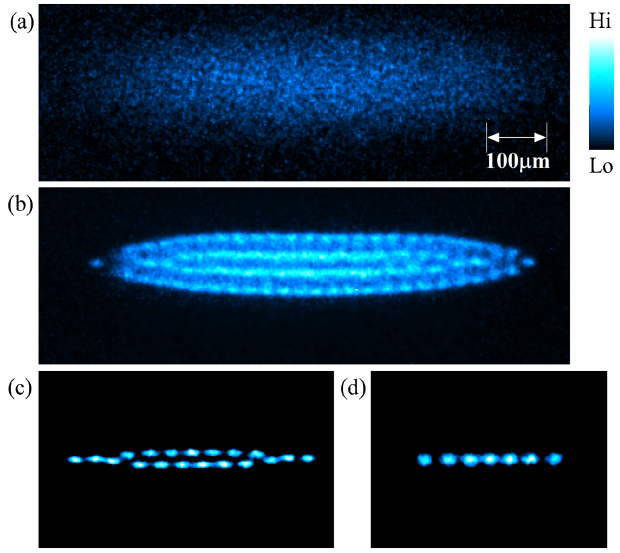

Fig. 8. (Color online) LIF images of $^{40}Ca^+$ ions detected by the ICCD camera with an exposure time of 0.8 s. (a) Ion cloud before laser cooling. (b) 3D "multishell" Coulomb crystal formed by several tens of ions. (b) 2D "zigzag" Coulomb crystal consisting of 19 ions. (d) 1D "string" crystal consisting of 7 ions.

forming a string crystal is small, the emittance growth is lightened, which supports the above expectation that inter-particle Coulomb forces are responsible for the heating.

4. Experiments

4.1 Production of Coulomb crystals

For the present purpose, we only need string Coulomb crystals consisting of a few $^{40}Ca^+$ ions. The electron beam from the gun, however, inevitably ionizes many neutral particles including not only Ca atoms from the oven but also residual gases in the chamber. To minimize these backgrounds, we first operate the LPT in the mass-filter mode; namely, DC biases of about ± 10 V are added to the quadrupole electrodes to shift the LPT operating point near the Mathieu's stability boundary. The rf amplitude and frequency are set at $V_{rf} = 85$ V and $f = 2$ MHz. Possible background ions could be removed with this parameter setup. After purifying the $^{40}Ca^+$ plasma, we shut down the electron beam and move the LPT operating point away from the stability boundary by dropping the bias voltage to zero and the rf amplitude to 30 V. An LIF image taken right after the ionization process is shown in Fig. 8(a) where the plasma temperature is several thousands of Kelvin. We can reduce the number of confined $^{40}Ca^+$ ions either by heating the plasma with a detuned laser or by quickly switching the end-plate voltage $V_{A(B)}$ on and off.

LIF signals from laser-cooled $^{40}Ca^+$ ions are shown in Figs. 8(b)–8(d), where each spot represents a single $^{40}Ca^+$ ion. The structure of a Coulomb crystal depends on the total ion number N_i, and the transverse and longitudinal focusing forces. Under the experimental conditions outlined above ($f = 2$ MHz, $V_{rf} = 30$ V, $V_A = V_B = 0.5$ V), a string crystal is transformed to the zigzag configuration when N_i exceeds 9. The crystalline states are quite stable and last for an extremely long time. According to our past experiences, the lifetime of a crystal is shortened if we omit the mass selection procedure.

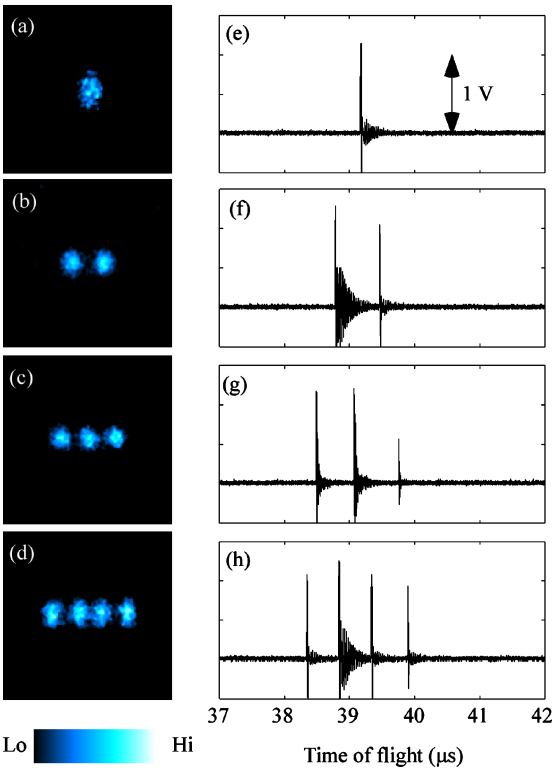

Fig. 9. (Color online) LIF images of Coulomb crystals before extraction (left panels) and the corresponding signals output from the MCP. The origin of the abscissa (TOF) is the moment when we switch the end-plate voltages V_A and V_B.

4.2 Extraction of ultracold ions

A number of string-crystal extraction experiments have been carried out with various setups of the system. Figure 9 gives several examples of MCP output signals obtained under the same conditions, as assumed in the numerical simulation of Fig. 5. A similar measurement result has been

given in ref. 23. The four left panels show LIF images of Coulomb crystals before extraction. Each crystal is axially released toward the MCP when the end-plate voltages are switched from 0.5 V to $V_A \to 0$ V and $V_B \to 20$ V ($U_A = 0$ V and $U_B = 20$ V) within 10 ns. The MCP signals on the right panels clearly indicate that the ultracold ions can be transported keeping equal time intervals. The time of flight (TOF) with this setup is approximately 39 μs, which is in reasonable agreement with numerical estimates.

We have found that the number of spikes is not always consistent with the number of ultracold ions counted before the extraction, while all ions must reach the MCP according to detailed 3D simulations. The discrepancy is believed to come from the limitation of the MCP detector currently employed for the experiments.[30] In fact, the particle-detection efficiency of the MCP is approximately 60% according to the specifications. To confirm this, we repeated a single-ion extraction experiment maintaining all parameters. 29 clear events were then detected in 54 trials, which roughly agrees with the specifications.[31] We are now considering the replacement of the MCP with a higher-sensitivity detector to improve the quality of observable information.

4.3 *Control of TOF and time intervals of extracted ions*

In order to allow successive acceleration with an rf linac, the time structure of extracted ions must also be controllable. Otherwise, it becomes difficult to put each ion near a stable fixed point (Fig. 1). Serious axial heating of the beam might then be caused by the strong rf acceleration field. Here, we test the most straightforward scheme to achieve our goal; namely, we try to control the TOF and time intervals of the extracted ions simply by adjusting the switching voltages on the end plates. Although the importance of synchronization with the phase of the rf field in the LPT is emphasized in ref. 23, our system is insensitive to the timing of ion extraction. We have actually obtained similar results both experimentally and numerically even if the rf phase at the extraction is changed. In the experiments whose results are shown in Fig. 9, the end-plate voltages are switched at the moment when the rf potentials of all four quadrupole electrodes become zero. The same switching phase is used in the following experimental results.

Similarly to that in the experiments whose results are shown in Fig. 9, the end-plate voltages (V_A and V_B) was switched from 0.5 V to other final values (U_A and U_B) within 10 ns and the TOF (τ_{TOF}) to the MCP was measured. As in the numerical simulations given above, the DC voltage V_A on the end plate of the MCP side is always dropped to zero (i.e., $U_A = 0$). On the other hand, the final voltage U_B on the other end plate is varied over a wide range. As shown in Fig. 9 where U_B is fixed at 20 V, the average TOF over all extracted ions is almost independent of the initial ion number. We, therefore, checked the TOF of a single ultracold ion when it was launched with various values of U_B. The result is plotted in Fig. 10 as a function of U_B. The possible measurement errors should be less than ±7 ns. Naturally, τ_{TOF} becomes shorter as U_B is increased. τ_{TOF} is long when $U_B \approx 0$, because the axial potential well becomes flatter around the center of the LPT at the ion extraction. The broken curve in Fig. 10 indicates the corresponding simulation result that agrees well with the experimental observations.

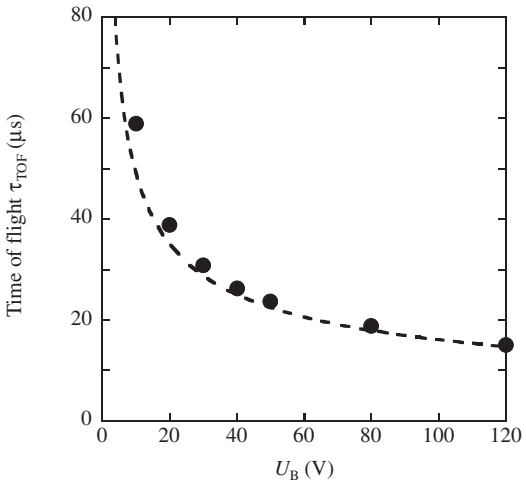

Fig. 10. Time of flight of an ultracold single ion versus the final voltage U_B of the end plate B. The end-plate voltage V_B is kept at 0.5 V during laser cooling and then switched to various final values (U_B) within 10 ns for ion extraction. The broken curve represents the corresponding simulation results. The possible errors in TOF measurements are less than ±7 ns.

Another key factor for the realization of the ultralow-emittance beam generator in Fig. 1 is the controllability of *time* intervals between neighboring ions. Controlling *spatial* intervals between extracted ions is trivial unless the kinetic energy of the beam is an issue; all we have to do is to accelerate the ions with a DC voltage after they come out of the trap.[21] This implies that we cannot handle the time intervals by simply accelerating or decelerating the ions by adjusting static potential after the extraction. We thus consider the use of U_B again and check if the time interval is adjustable in practice. Since U_B determines the axial gradient of the electrostatic extraction potential, the energy gain of an ultracold ion depends on its initial location and should be variable with U_B. Figure 11 shows the measured time interval $\Delta\tau$ of two laser-cooled ions when they arrive at the MCP. We confirm that $\Delta\tau$ can be controlled by adjusting the end-plate potential U_B. The broken curve is the result of numerical simulations based on exactly the same parameters as employed in the actual experiments; namely, we first cool hot ions assuming the actual experimental conditions, form a string Coulomb crystal, and then, extract it from the trap by switching the end-plate voltages. The experimental observations are again well explained by the simulations. We further give, in Fig. 12, the results of time-interval measurements when three ultracold ions are launched from the LPT. The time intervals between the first and second ions (black circles) and between the second and third ions (open circles) are measured at the MCP position with several different values of U_B. In all cases, three ions are almost equally spaced while travelling along the axis and arrive at the detector one after another. The two broken curves in Fig. 12, which are overlapping, correspond to the 3D simulation results.

5. Concluding Remarks

We have conducted an experimental study of a novel ion

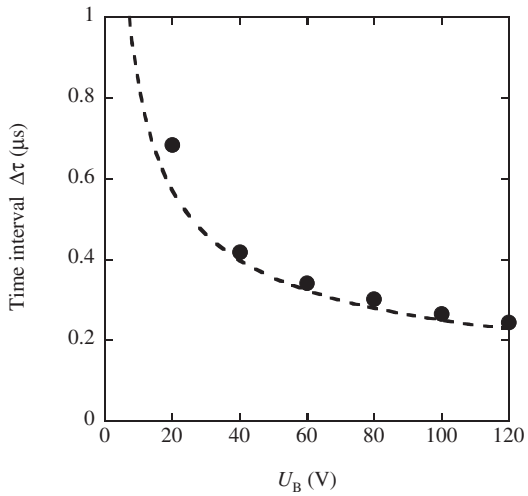

Fig. 11. U_B dependence of the time interval of two ultracold ions when they reach the MCP detector. The experimental conditions are identical to those adopted in Fig. 6 except that we have extracted two ions here instead of one. The broken curve represents the corresponding 3D simulation results.

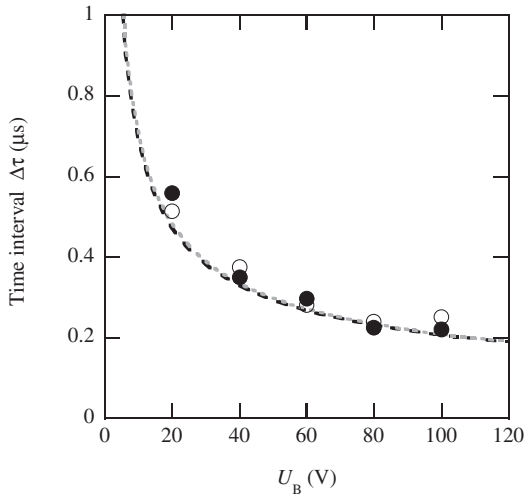

Fig. 12. U_B dependence of the time intervals of three ultracold ions when they reach the MCP detector. The experimental conditions are identical to those adopted in Fig. 6 except that we have extracted three ions here instead of one. The black circles correspond to the measured time intervals $\Delta\tau$ between the first and second ions at the MCP, while the open circles to $\Delta\tau$ between the second and third ions. The two broken curves overlapping with each other show the 3D simulation results in which the same conditions as those used in the experiments are assumed.

source that can, in principle, generate ultralow-emittance beams of arbitrary kinetic energies. The core of the system is a compact LPT where a small number of ions are manipulated with laser light before the extraction. The LPT employed here is quite conventional, which consists solely of four cylindrical rods and two end plates. In order to verify the possibility of using such a simple device for micro- or even nano-beam production, systematic experiments are carried out under various conditions. It is demonstrated that the nondestructive extraction of a string Coulomb crystal is feasible simply by switching the DC voltages on the end plates. We have further confirmed the controllability of the two key parameters that justifies the concept of the ultralow-emittance beam generator in Fig. 1; one essential parameter is the TOF of an ultracold ion and the other the time intervals of adjacent ions. If these parameters are adjustable, the rf heating effect during acceleration to a very high energy can be minimized, at least, in theory. The experimental results in §4, which agrees with the results of the corresponding 3D numerical simulations, indicate that both TOF and time interval can be controlled by adjusting the extraction voltage U_B. Although the attainable beam intensity is limited, all fundamental information is known in advance including the exact number of ions in the beam, precisely when they are arriving at a target, and how much they are distanced in time and space. The kinetic energy of each individual ion is also known at high precision. The possible normalized transverse emittance can be on the order of 10^{-13} m, far below the level of common low-intensity ion beams. Even lower emittances are achievable by cooling the ions to the motional ground state[23] or by optimizing the design parameters of the system. Although further systematic experimental and numerical studies are necessary, the present results look quite encouraging as a starting point toward the realization of practical nanobeam generators.

An easy future improvement of our system includes a slight modification of the electrode configuration. The current LPT is composed of long quadrupole rods and two end plates [see Fig. 3(a)], but it is useful to divide the rods axially into several pieces, instead of using the end plates, so that we can form a couple of potential wells along the LPT axis by independently biasing the electrodes.[32] Such a "multisection" LPT makes it possible for us to separate the laser-cooling and ionization regions. The separation of the two regions is advantageous in eliminating the unwanted side effect caused during the ionization process. In Figs. 10 and 11, we recognize a slight discrepancy between the experiment and simulation results when U_B is low. We believe that this is due mainly to the contamination of the electrodes by high-temperature Ca gases from the oven. The effect of the contaminant on the electrode surfaces is weak but finite, which possibly induces a non-negligible distortion of the ion-extraction potential especially in a low-U_B range. We expect that the multisection LPT under consideration will resolve this problem and improve the controllability of extracted particles.

Acknowledgments

This work was supported in part by a Grant-in-Aid for Scientific Research from the Japan Society for the Promotion of Science and by the High Energy Accelerator Research Organization. The authors would like to thank K. Toyoda of Osaka University for stimulating discussions and assistance in developing the laser cooling system.

1) G. Dollinger, V. Hable, A. Hauptner, R. Krücken, P. Reichart, A. A. Friedl, G. Drexler, T. Cremer, and S. Dietzel: Nucl. Instrum. Methods Phys. Res., Sect. B **231** (2005) 195.
2) Y. Kobayashi, T. Funayama, S. Wada, M. Taguchi, and H. Watanabe: Nucl. Instrum. Methods Phys. Res., Sect. B **210** (2003) 308.
3) K. M. Prise, M. Folkard, and B. D. Michael: Radiat. Prot. Dosim. **104** (2003) 347.
4) T. Hirao, H. Mori, J. S. Laird, S. Onoda, T. Wakasa, H. Abe, and H.

Itoh: Nucl. Instrum. Methods Phys. Res., Sect. B **210** (2003) 227.
5) D. H. Cho, Y. Suzuki, M. Tanaka, M. Hachiro, and K. Pak: J. Cryst. Growth **237–239** (2002) 1455.
6) Q. Ji, K.-N. Leung, T.-J. King, X. Jiang, and B. R. Appleton: Nucl. Instrum. Methods Phys. Res., Sect. B **241** (2005) 335.
7) Y. Lee, Q. Ji, K. N. Leung, and N. Zahir: Rev. Sci. Instrum. **71** (2000) 722.
8) J. Orloff: Rev. Sci. Instrum. **64** (1993) 1105.
9) B. Tomiyasu, I. Fukuju, H. Komatsubara, M. Owari, and Y. Nihei: Nucl. Instrum. Methods Phys. Res., Sect. B **136–138** (1998) 1028.
10) A. Lamperti, C. E. Bottani, P. M. Ossi, and R. Levi-Setti: Surf. Coat. Technol. **180–181** (2004) 323.
11) H. D. Wanzenboeck, C. Ostermaier, A. Gruen, B. Eichinger, M. Karner, and E. Bertagnolli: Nucl. Instrum. Methods Phys. Res., Sect. B **242** (2006) 257.
12) The emittance of a beam is defined as the volume occupied by the beam in a six-dimensional (6D) phase space. The beam extent of a particular spatial direction is related to the projection of the 6D volume onto that direction. The emittance is roughly unchanged in a conservative dynamical system; magnets and other beam focusing devices never change the emittance. In order to reduce the emittance without particle losses, we need some dissipative mechanism such as laser cooling.
13) Y. Iwai, T. Ikeda, T. M. Kojima, and Y. Yamazaki: Appl. Phys. Lett. **92** (2008) 023509.
14) M. Oikawa, T. Satoh, T. Sakai, N. Miyawaki, H. Kashiwagi, S. Kurashima, S. Okumura, M. Fukuda, W. Yokota, and T. Kamiya: Nucl. Instrum. Methods Phys. Res., Sect. B **260** (2007) 85.
15) R. P. Ghosh: *Ion Traps* (Oxford Science, Oxford, U.K., 1995), and references therein.
16) D. J. Berkeland, J. D. Miller, J. C. Bergquist, W. M. Itano, and D. J. Wineland: Phys. Rev. Lett. **80** (1998) 2089.
17) M. Block, A. Drakoudis, H. Leuthner, P. Seibert, and G. Werth: J. Phys. B **33** (2000) 375.
18) N. Kjærgaard, L. Hornekær, A. M. Thommesen, Z. Videsen, and M. Drewsen: Appl. Phys. B **71** (2000) 207.
19) R. W. Hasse and J. P. Schiffer: Ann. Phys. (N.Y.) **203** (1990) 419.
20) A. Ogata and H. Okamoto: in *Quantum Aspects of Beam Physic*, ed. P. Chen (World Scientific, Singapore, 2000) p. 269.
21) M. Kano, S. Masuda, A. Ogata, K. Okabe, and H. Okamoto: J. Phys. Soc. Jpn. **73** (2004) 760.
22) K. Izawa, H. Higaki, H. Yamate, H. Hitomi, K. Ito, M. Kuriki, and H. Okamoto: J. Phys.: Conf. Ser. **163** (2009) 012102.
23) W. Schnitzler, N. M. Linke, R. Fickler, J. Meijer, F. Schnidt-Kaler, and K. Singer: Phys. Rev. Lett. **102** (2009) 070501.
24) The ions do not necessarily occupy consecutive fixed points but can be placed on every n fixed points, where n is an arbitrary positive integer.
25) T. Hänsch and A. Schawlow: Opt. Commun. **13** (1975) 68.
26) D. J. Wineland and H. Dehmelt: Bull. Am. Phys. Soc. **20** (1975) 637.
27) For more information, see http://www.cst.com/Content/Products/CST_S2/overview.aspx
28) A string Coulomb crystal is generally more stable than the other multidimensional crystalline structures. A wider range of choices can, therefore, be made for the rf amplitude.
29) See, for example, *Handbook of Accelerator Physics and Engineering*, ed. A. W. Chao and M. Tigner (World Scientific, Singapore, 1999).
30) The effect of limited detector efficiency on measurement results has also been mentioned in ref. 23.
31) This suggests that the present system might be usable to calibrate MCPs and the electron multiplier tubes at high precision.
32) R. Takai, H. Enokizono, K. Ito, Y. Mizuno, K. Okabe, and H. Okamoto: Jpn. J. Appl. Phys. **45** (2006) 5332.